Biogeosciences Discuss., 12, 12611–12651, 2015
www.biogeosciences-discuss.net/12/12611/2015/
doi:10.5194/bgd-12-12611-2015

Biogeosciences Discussions
Open Access

Influence of timing of sea ice retreat on phytoplankton size during marginal ice zone bloom period in the Chukchi and Bering shelves

A. Fujiwara[1], T. Hirawake[2], K. Suzuki[3], L. Eisner[4], I. Imai[2], S. Nishino[1], T. Kikuchi[1], and S. I. Saitoh[2]

[1]Institute of Arctic Climate and Environment Research, Japan Agency for Marine-Earth Science and Technology, 2-15, Natsushima, Yokosuka, Kanagawa, Japan
[2]Faculty/Graduate School of Fisheries Sciences, 3-1-1 Minatocho, Hakodate, Hokkaido 041-8611, Japan
[3]Faculty of Environmental Earth Science, Hokkaido University/JST-CREST, N10 W5, Kita-ku, Sapporo, Hokkaido 060-0810, Japan
[4]Alaska Fisheries Science Center, National Marine Fisheries Service, (NOAA), 7600 Sand Point Way, Seattle WA, USA

Received: 16 April 2015 – Accepted: 16 July 2015 – Published: 10 August 2015

Correspondence to: A. Fujiwara (amane@jamstec.go.jp)

Published by Copernicus Publications on behalf of the European Geosciences Union.

BGD
12, 12611–12651, 2015

Abstract

Timing of sea ice retreat (TSR) as well as cell size of primary producers (i.e., phytoplankton) plays crucial roles in seasonally ice-covered marine ecosystem. Thus, it is important to monitor the temporal and spatial distribution of phytoplankton community size structure. Prior to this study, an ocean color algorithm has been developed to derive phytoplankton size index F_L, which is defined as the ratio of chlorophyll *a* derived from the cells larger than 5 µm to the total chl *a* using satellite remote sensing for the Chukchi and Bering shelves. Using this method, we analyzed pixel-by-pixel relationships between F_L during marginal ice zone (MIZ) bloom period and TSR over a period of 1998–2013. The influence of TSR on sea surface temperature (SST) and changes in ocean heat content (ΔOHC) during the MIZ bloom period were also investigated. A significant negative relationship between F_L and TSR was widely found in the shelf region during MIZ bloom season. On the other hand, we found a significant positive (negative) relationship between SST (ΔOHC) and TSR. That is, earlier sea-ice retreat was associated with a dominance of larger phytoplankton during a colder and weakly stratified MIZ bloom season, suggesting that duration of nitrate supply, which is important for large-sized phytoplankton growth in this region (i.e., diatoms), can change according to TSR. In addition, under-ice phytoplankton blooms are likely to occur in years with late ice retreat, because sufficient light for phytoplankton growth can pass through the ice and penetrate into the water columns due to an increase in solar radiation toward the summer solstice. Moreover, we found not only the length of ice-free season but also annual median of F_L positively correlated with annual net primary production (APP). Thus, both phytoplankton community composition and growing season are important for APP in the study area. Our findings showed quantitative relationship between the inter-annual variability of F_L, TSR and APP suggesting satellite remote sensing of phytoplankton community size structure is suitable to document the impact of recent rapid sea ice loss on ecosystem of the study region.

BGD
12, 12611–12651, 2015

1 Introduction

The widely spread continental shelf from the northern Bering Sea to the southern Chukchi Sea in known as one of the most biologically productive regions in the world ocean (Springer and McRoy, 1993). Nutrient rich water forms during wintertime as a consequence of strong vertical mixing, and it supports extremely high primary productivity from spring to fall (Springer and McRoy, 1993). The high primary production in the region is not completely consumed by the grazers in the water column due to low grazing pressure, fast sinking rate of large chain-forming diatoms and shallow bottom depths (Grebmeier et al., 1988, 2006a). As a result, this region supports a large amount of benthic biomass, and subsequently, top predators such as walrus (*Odobenus rosmarus*), gray whale (*Eschrichtius robustus*) and various sea birds also gather to feed on the rich benthic ecosystem (Sheffield et al., 2001; Moore et al., 2003; Feder et al., 2005). Thus, the marine ecosystems in this region have been characterized by rather short food webs and efficient energy transport to higher trophic levels through tight pelagic-benthic coupling (Grebmeier and Dunton, 2000). However, recent sea ice decline and ocean warming in the northern Bering Sea triggered the northward shift of this tightly coupled pelagic-benthic ecosystem (Grebmeier et al., 2006b). Ocean warming can modify the ecosystem structure from a pelagic-benthic to a pelagic-pelagic type that is generally found in the southern region (Piepenburg, 2005). Marine ecosystems in the northern Bering and Chukchi Seas are now facing extreme climate change, thereby, it is important to improve our comprehension of how the ecosystems respond to environmental change. Several studies have already reported that the changes in mammals, sea birds and benthic species composition and distribution were found in the Chukchi Sea (Grebmeier et al., 2012 and references there in), though studies on the changes in phytoplankton taxa are relatively scarce. Since even the small changes in lower trophic levels can greatly affect higher trophic level organisms through the efficient and short energy transfer pathway of the arctic marine ecosystems (Grebmeier

BGD
12, 12611–12651, 2015

et al., 2010), it is essential to clarify how primary producers (i.e., phytoplankton) respond to recent environmental changes in terms of their size structure and productivity.

Satellite ocean color remote sensing has enabled us to monitor spatial and temporal dynamics of marine phytoplankton in diverse ecosystems. Several studies have attempted to measure not only chlorophyll *a* (chl *a*) and primary productivity over the euphotic zone (PP_{eu}) but also phytoplankton functional types (PFTs) from space (e.g., Alvain et al., 2005; Uitz et al., 2006; Kostadinov et al., 2009; Brewin et al., 2010; Hirata et al., 2011). Satellite remote sensing of PFTs is a powerful way to assess biological contributions to biogeochemical cycles and ecosystem variability over large spatial scales and continuous temporal scales. For example, Takao et al. (2012) found a significant relationship between inter-annual variability of phytoplankton community composition and primary production in the Indian sector of the Southern Ocean. Hirata et al. (2013) showed the potential of long-term monitoring of ecological provinces using satellite derived PFTs and marine ecosystem model derived PFTs at the global scale. Thereby, satellite remote sensing of PFT is expected to contribute to understanding of phytoplankton dynamics in the Chukchi and Bering Seas. However, the Chukchi and Bering Seas are known as optically complex waters and their optical properties are quite different from global pelagic waters; large proportions of colored dissolved organic matter (CDOM) absorption and highly packaged phytoplankton absorption cause large estimation errors in ocean color products (Matsuoka et al., 2007; Naik et al., 2013). To overcome the problems, use of regionally optimized ocean color algorithms instead of globally developed algorithms are required to accurately monitor chl *a*, PFT and euphotic-depth-integrated primary production (PP_{eu}). Cota et al. (2004) successfully modified a chl *a* algorithm to estimate chl *a* for highly packaged high latitude phytoplankton from space. Regionally optimized PFT algorithms for the Chukchi and Bering Seas were proposed by Fujiwara et al. (2011) to estimate the percent contribution of $> 5\,\mu m$ algal cells to total chl *a* biomass as an index for phytoplankton community size structure (hereafter F_L). The algorithm to derive PP_{eu} was also optimumly developed by Hirawake et al. (2012) for the western Arctic seas. Application of these regional

BGD
12, 12611–12651, 2015

ocean color algorithms to long time series satellite data is expected to contribute to comprehension of ecosystem changes.

In this study we focus on the timing of sea ice retreat (TSR) and phytoplankton size composition in the marginal ice zone (MIZ), which is the area where ice melt has just recently occurred. It has been shown that TSR can alter phytoplankton community composition in the northern Chukchi Sea in late summer (Fujiwara et al., 2014). However, little is known about the relationship between TSR and phytoplankton size composition in the shelf region of Bering and Chukchi Seas, nor during the spring phytoplankton bloom period. Spring phytoplankton blooms generally occur in the MIZ in the Arctic Ocean (Kahru et al., 2011; Perrette et al., 2011). Since phytoplankton grazers efficiently use the high phytoplankton biomass produced during bloom periods for their growth and production (e.g., Hunt et al., 2002, 2011; Søreide et al., 2011), the influence of TSR on phytoplankton size composition during the MIZ bloom period is crucial to understand to evaluate bottom-up effects of primary production on the food web. In this study, we aim to clarify the relationships between the temporal and spatial distribution of phytoplankton size composition and the marine environment during the MIZ bloom periods using satellite remote sensing. Secondly, we also aim to assess how phytoplankton size contributes to annual net primary production (APP).

2 Materials and methods

2.1 Satellite data

Satellite derived Level-2 and Level-3 standard mapped images of the daily ocean color dataset were obtained from GSFC/DAAC NASA (1 and 9 km resolution, respectively). Level-2 images were used to evaluate the satellite data model performance. To analyze longer and continuous time-series data (1998–2013), we used SeaWiFS and Aqua-MODIS Level-3 data. Remote sensing reflectance ($R_{rs}(\lambda)$, $\lambda = 412$, 443, 490, 555, and 670 nm for SeaWiFS and 412, 443, 488, 555, and 667 nm for Aqua-MODIS),

BGD
12, 12611–12651, 2015

euphotic depth (Z_{eu}) derived from the quasi-analytical algorithm (QAA) proposed by Lee et al. (2007), and photosynthetic available radiation (PAR) were downloaded. Reprocessing versions for the products were 2010.0 and 2013.1 for SeaWiFS and Aqua-MODIS, respectively. $R_{rs}(\lambda)$ for SeaWiFS were converted into $R_{rs}(\lambda)$ for MODIS with conversion factors that remove the biases between them (see appendix A). Definitions of the symbols are listed in Table 1.

Satellite-observed sea ice concentration (SIC) and sea surface temperature (SST) were used to assess the environmental conditions in the region. The Special Sensor Microwave Imager-Defense Meteorological Sattellite Program (SSMI-DMSP) derived SIC generated with the NASA-Team algorithm 2 (Markus and Cavalieri, 2000) was downloaded from the National Snow and Ice Data Center (NSIDC). The temporal and spatial resolutions were daily and 25 km, respectively. Following Perrette et al. (2011), nearest-neighbor interpolation was performed to the SIC dataset to convert 25 km spatial resolution into 9 km, so data were on the same scale as the ocean color images. AVHRR-derived SST was downloaded from the Physical Oceanography Data Active and Archive Center (PODAAC) for 1998–2012 and Aqua-MODIS derived SST was obtained from GSFC/DAAC NASA for 2003–2013 to cover the ocean color time-series.

2.2 Calculation of heat flux

Development of thermal stratification is a major controlling factor of nutrient supply into the upper layer from spring to summer seasons both in the Bering and Chukchi Seas (e.g., Hill et al., 2005; Coyle et al., 2008; Sambrotto et al., 2008). To understand how thermal stratification develops corresponding to yearly change of sea ice retreat timing in the region, changes of ocean heat content (ΔOHC) during the MIZ bloom season (see Sect. 2.3) were used as a proxy of surface mixed layer depth development. ΔOHC

BGD
12, 12611–12651, 2015

was calculated following the equation of Mizobata et al. (2012):

$$\Delta\mathrm{OHC} = \int_{\mathrm{TSR}}^{\mathrm{TSR+14}} (\mathrm{SHTFL} + \mathrm{LHTFL} + \mathrm{NSWRS} + \mathrm{NLWRS}), \quad (1)$$

where SHTFL, LHTFL, NSWRS and NLWRS are sensible heat flux, latent heat flux, net shortwave radiation and net longwave radiation, respectively. All products used in Eq. (1) were obtained from NCEP/NCAR daily reanalysis dataset (Kalnay et al., 1996). These Gaussian gridded reanalysis products were regridded into polar-stereographic projections and then interpolated into 9 km resolution by the nearest-neighbor method to achieve the same resolution as the satellite products.

2.3 Data processing

Chlorophyll *a* concentration (chl *a*) was computed by the Arctic-OC4L algorithm proposed by Cota et al. (2004) that optimized for optical properties of phytoplankton in the Arctic Ocean:

$$\text{chl } a = 10^{0.592-3.607R}, \quad (2)$$

where R is the maximum band ratio defined as $\log(R_{rs}[443] > R_{rs}[490]/R_{rs}[555])$ for SeaWiFS and $\log(R_{rs}[443] > R_{rs}[488]/R_{rs}[555])$ for MODIS. The original Arctic-OC4L algorithm uses $R_{rs}(510)$, though we did not use this band because there is no observation band around 510 nm in MODIS. We found there was no statistically significant difference in chl *a* with or without inclusion of $R_{rs}(510)$ (data not shown).

An index for the phytoplankton community size composition (F_L) was defined as the ratio of chl *a* attributed to cells larger than 5 µm (chl $a_{>5\,\mu m}$) to total chl *a* (chl a_{total}):

$$F_L = \text{chl } a_{>5\mu m}/\text{chl } a_{total}. \quad (3)$$

BGD
12, 12611–12651, 2015

Satellite F_L was estimated by the phytoplankton size derivation model (SDM) proposed in Fujiwara et al. (2011) that optimized for the phytoplankton communities and the optical properties in the Bering and Chukchi Seas. The SDM requires the ratio of the phytoplankton absorption coefficient ($a_{ph}(\lambda)$) and spectral slope of the particle backscattering coefficient (γ) to compute F_L. $a_{ph}(\lambda)$ was calculated by the QAA version 5 (QAA v-5) (Lee et al., 2009), but spectral slope of the absorption coefficient of gelbstoff + detritus (S_{dg}) was modified for the region (Appendix B) to avoid the retrieval of negative $a_{ph}(\lambda)$. γ was empirically quantified using the $R_{rs}(\lambda)$ ratio (Fujiwara et al., 2011). Then, F_L can be derived by Eq. (4):

$$F_L = \frac{1}{1 + \exp[-(X_0 + X_1 \cdot a_{ph}(\lambda_1)/a_{ph}(\lambda_2) + X_2 \cdot \gamma)]}, \quad (4)$$

where, $X_0 = 3.175$, $X_1 = -0.570$ and $X_2 = -0.565$, and $\lambda_1 = 488$ and $\lambda_2 = 555$.

Euphotic-depth-integrated primary production (PP_{eu}) was derived by the Absorption Based Productivity Model (ABPM) proposed in Hirawake et al. (2011, 2012). The ABPM is originally based on a vertically generalized productivity model (VGPM) (Behrenfeld and Falkowski, 1997) but ABPM retrieves optimal values of chl *a* normalized productivity (P^B_{opt}) from $a_{ph}(\lambda)$ instead of from SST and chl *a*. The use of $a_{ph}(\lambda)$ is suitable to discuss the effect of ocean warming on PP_{eu}, because PP_{eu} by ABPM is independently derived from temperature (Hirawake et al., 2011). ABPM also effectively reduces the optical effect of high CDOM water in the study region via its calculation steps of $a_{ph}(\lambda)$ using QAA (Hirawake et al., 2012). PP_{eu} using ABPM was determined with the following equations:

$$PP_{eu} = P^B_{opt} \cdot \text{chl } a \cdot 0.66125 \cdot E_0/(E_0 + 4.1) \cdot Z_{eu} \cdot DL, \quad (5)$$

and,

$$P^B_{opt} \cdot \text{chl } a = 102.44 \cdot a_{ph}(443)^{1.431}, \quad (6)$$

BGD
12, 12611–12651, 2015

where E_0 and DL indicate daily surface photosynthetically available radiation and day length, respectively. DL was computed from date and latitude following the method of Brock (1981).

Since ocean color products can only be retrieved from cloud- and ice-free pixels in the satellite imagery, we computed 9 day moving average for $a_{ph}(443)$ and Z_{eu} to increase retrievals of valid PP_{eu}. We also applied nearest-neighbor spatial interpolation to the daily satellite images. TSR was calculated using daily SIC data for each year. In this study, non-ice covered pixels were defined as SIC < 10 % following Pabi et al. (2008), and TSR was defined as the last date when the SIC falls below 10 %, prior to observed annual sea ice minimum across the study region during summer (50–75° N, 170–210° E).

Perrette et al. (2011) have shown that high chl *a* values occur during the MIZ bloom period, which is defined as 20 days after sea ice melt in ~ 90 % of the Arctic Ocean. On the other hand, Niubauer et al. (1991) reported that the sea ice related spring bloom lasts for ~ 2 weeks on the Bering Sea shelf unless there is a mixing event. To clarify the relationship between TSR and phytoplankton size composition during the bloom period, we computed 14 day averages of the variables (F_L, SST and PAR) after sea ice melted for each pixel, and defined them as the MIZ bloom period values. Then, correlation analysis (Spearman's rank correlation coefficient, ρ) was conducted to evaluate interannual variations between the MIZ bloom time variables and TSR for every one-by-one pixel. Note that spatial statistical analysis was conducted only for the regions where sea ice was observed in at least 11 of the 16 years.

Standardized multiple regression analysis was also performed to determine what variables contributed to inter-annual variability of annual primary production (APP). APP was computed by integrating PP_{eu} for every non-ice covered pixel. Annual median PP_{eu} was calculated for each pixel, and was substituted to compute accurate APP when PP_{eu} was missed due to cloud cover. Then, APP was regressed using annual median F_L, SST and length of open water period for every one-by-one pixel:

$$\mathrm{APP} = A_1 \cdot \mathrm{OWP} + A_2 \cdot F_L + A_3 \cdot \mathrm{SST}, \quad (7)$$

BGD
12, 12611–12651, 2015

where A_1, A_2 and A_3 indicate partial regression coefficients, and OWP denotes the length of open water period (i.e., the number of non-ice covered days). All variables were standardized before conducting multiple regression analysis by subtracting by the climatological mean and dividing by the SD. Thus, contribution of the variables of Eq. (7) to APP is comparable to using partial regression coefficients. Note that the multiple regression analysis was performed for areas that seasonal ice cover had been observed in every year. MATLAB statistical toolbox (The Math Works, Inc.) was used for the statistical analyses of this study.

2.4 In situ data sampling for the evaluation of satellite products

In situ total and size-fractionated chl *a* samples was obtained during the cruises of Bering Arctic SubArctic Integrated Survey (BASIS) program conducted in late summer to fall (August to October) of 2005, 2006, and 2007, and the cruises of GRENE Arctic Climate Change Research Project conducted in late summer to fall of 2012 (September to October) and early summer of 2013 (June to July) on the Bering and Chukchi shelves (Fig. 1). For these samples, 138–525 mL of seawater were filtered onto 10, 5, 2 µm pore-sized nuclepore polycarbonate filters and GF/F filters. All chlorophyll samples were frozen at onboard, stored in liquid nitrogen or in a supercold freezer (−80 °C) (except during 1–2 days when samples were shipped in coolers on ice) and analyzed later (within 1–8 months) using the acidification technique (Parsons et al., 1984) with a Turner Designs 700 fluorometer for the samples from BASIS cruises and non-acidification technique (Welshmeyer et al., 1994) with a Turner Designs 10-AU fluorometer for the samples from the GRENE cruises. While different chl *a* measurement methods were performed between the cruises, the fluorometers were calibrated with a pure chl *a* standard prior to analysis to minimize the difference between the cruises. Then, in situ F_L was calculated from Eq. (3) and compared with daily matched-up satellite derived F_L (MODIS L2). Root mean square error between satellite derived F_L and in situ measured F_L was calculated to evaluate the SDM performance.

BGD
12, 12611–12651, 2015

In situ primary productivity (PP) data, as well as chl *a*, was also used to assess the influence of sub-surface chl *a* maximum (SCM) on remotely estimated PP_{eu}. PP samples were collected during the cruises of T/S *Oshoro-maru* (Hokkaido University, IPY and GRENE cruise) and R/V *Mirai* (JAMSTEC, GRENE cruise) in the same region with chl *a* samples (Fig. 1). Cruises were conducted in early summer to fall (June to October) of 2007, 2008, 2012 and 2013. PP was measured for several optical depths and then PP_{eu} was calculated integrating PP from surface to Z_{eu} (See Hirawake et al., 2012 for more details of the sampling and analysis).

3 Results

3.1 Evaluation of performance of the satellite algorithms

Accuracy of the SDM-derived F_L was evaluated by comparing F_L from in situ measurements and the daily matched-up MODIS Level-2 dataset. Twenty-five data points were available for this examination widely collected in the Bering Sea and Chukchi Sea during different seasons (Fig. 1). Figure 2a compares the satellite derived F_L and in situ F_L. SDM successfully retrieved F_L for 15 of 22 data points (68 % of data) within ±20 % F_L range (Fig. 2a). RMSE was 25 %. The satellite validation was quite similar to the result of Fujiwara et al. (2011) who showed that the derived F_L using in situ measured $R_{rs}(\lambda)$ had a 69 % accuracy and RMSE = 22.7 %. Although we found a slight overestimation in the low F_L range and slight underestimation in the high F_L range, the high determination coefficient indicates the correlation is sufficient to address the variability of F_L. Here we conclude that SDM is applicable to satellite remote sensing in the Bering and Chukchi Seas, and SDM is well optimized for what is known as optically complex water (Matsuoka et al., 2007; Naik et al., 2013).

To confirm how satellite derived F_L and PP_{eu} represent water column phytoplankton size structure and productivity, we compared surface and vertical mean F_L (averaged F_L from 0–50 m) using in situ dataset (Fig. 2b). Vertical mean F_L shows significant

BGD
12, 12611–12651, 2015

relationship with surface F_L ($r^2 = 0.73$, $p < 0.01$) in spite of the presence of SCM in the many sampling sites. Similarly, PP_{eu} also significantly correlated with surface PP (Fig. 2c), suggesting the large contribution of surface primary production to PP_{eu}. Although both surface value of F_L and PP explain the water column average and the integrated values, the depth of PP maximum (6.1 ± 8.9 m) was significantly shallower than the depth of chl *a* maximum (20.1 ± 13.7 m) (Fig. 2d).

3.2 Timing of the open water bloom

In order to determine the timing of the spring phytoplankton bloom, we investigated the relationship between TSR and date of occurrence of the yearly chl *a* maximum (CMAX). Figure 3a denotes the climatologic median of TSR from 1998–2013. It indicates sea ice normally retreats by summer solstice except in the northwestern edge of the study area. Timing of CMAX showed a similar spatial pattern to TSR (Fig. 3b) except for coastal Alaska such as in Kotzebue Sound and Norton Sound. In those areas, CMAX occured in late summer. However, CMAX generally occurs immediately after the sea ice retreat (less than ~ 20 day after sea ice retreat) in almost the entire shelf area (Fig. 3c). However, the CMAX date was delayed near the Alaska coast, where Alaska Coastal Water usually flows, and in the western Bering Strait. In such regions, the timing of CMAX compared to TSR exceeds 50 days.

3.3 Influence of TSR on phytoplankton size composion during the MIZ blooms

Spearman's rank correlation coefficient was calculated for every one-by-one pixel between F_L and TSR, SST and TSR, ΔOHC and TSR, and PAR and TSR (Fig. 4a–d). Proportions of statistical significance of ρ were listed in Table 2. We found F_L during the bloom period negatively associated with TSR in 68 % of the shelf area with 15 % of the area significantly correlated ($p < 0.05$). A significantly positive ($p < 0.05$) relationship was found for the western side of the Bering Strait and western coast of Alaska; this area accounted for 2 % of the whole study area. SST during the MIZ bloom period

BGD
12, 12611–12651, 2015

was tightly and positively correlated with TSR over most (92 %) of the region (Fig. 4b): with 65 % significantly correlated. ΔOHC also had a similar but inverse spatial pattern with SST, with a statistically significant negative relationship over 61 % of the area (Fig. 4c). These results reveal that earlier sea ice retreat is associated with cold surface temperature and a relatively large amount of heat release from the sea surface during the MIZ bloom period. However, on the northwestern edge of the Chukchi Sea correlations were in the opposite direction with significantly positive ρ between SST and TSR, and significantly negative ρ between ΔOHC and TSR (Fig. 4b and c). PAR was strongly and positively correlated with TSR for the northern Bering Sea up to through the Bering Strait, but became negative in the northern part of the Chukchi Sea shelf (Fig. 4d). The highest positive ρ between PAR and TSR was found where sea ice normally retreats before the summer solstice, the time when the largest daily PAR would be observed (Fig. 3a).

3.4 Factors controlloing annual net primary production

Standardized multiple regression analysis was used to determine the contribution of controlling factors for APP. Here we compared the partial regression coefficients for annual median values of length of open water period, F_L, and SST to determine the contribution to inter-annual change in APP. Spatial distribution of partial regression coefficients for each variable are shown in Fig. 5a–c. All variables had positive coefficients for most of the study region. Accordingly, APP was also successfully modeled ($p < 0.05$, F test) using these variables in all regions except for the Gulf of Anadyr and coastal Alaska (Fig. 5d). This analysis revealed that longer growing seasons, larger proportions of large sized phytoplankton assemblages, and higher SSTs generally enhance APP. However, the magnitude of the contribution changes regionally. Larger partial regression coefficients for length of open water period (> 0.7) were found mainly in the northern shelf area of the Chukchi Sea (Fig. 5a). Larger partial regression coefficients for F_L (> 0.7) were mainly found on the Bering Sea shelf and part of the central Chukchi Sea shelf (67–70° N, 170–175° W) where other variables showed relatively

BGD
12, 12611–12651, 2015

lower contributions (Fig. 5b). On the other hand, the partial regression coefficients for SST were negative on the southern edge of the Bering Sea shelf study area (Fig. 5c). According to the standardized multiple regression analysis, in regions with seasonal ice cover large phytoplankton positively contribute to APP on the northern Bering Sea shelf and a longer open water period is a major factor for APP in the Chukchi Sea shelf.

4 Discussion

4.1 Evaluation of performance of the satellite algorithms

Validation of satellite derived F_L showed sufficient correlation with in situ F_L, though vertical distribution of phytoplankton should be confirmed, because SCM commonly distributes in the study area and high Arctic Ocean (e.g., Hill et al., 2005; Ardyna et al., 2013). The omission of SCM sometimes causes large error in satellite estimation of PP_{eu} in high Arctic Ocean (Hill et al., 2013). However, our results indicated both surface F_L and PP represent water column mean or integrated values. Similarly, Lomas et al. (2012) showed quite good relationship between surface chl *a* and euphotic zone integrated chl *a* for the Bering shelf. Thereby, we suggest surface F_L can be reasonably used to predict upper layer phytoplankton size structure as well. It might be due to the shallow bathymetry and SCM depth (~ 20 m) associated with nitracline depth (Brown et al. in-press) compared to higher Arctic Ocean where deeper SCM (> 40 m) is commonly found (Ardyna et al., 2013). Furthermore, significant shallower depth of PP maximum than the depth of SCM (Fig. 2d) causes smaller contribution of PP at SCM to PP_{eu}. This is consistent with Brown et al. (2015) has shown for the Chukchi shelf. Hence, we believe that use of ocean color remote sensing is applicable to discuss the temporal and spatial relationship between the distribution of sea ice and phytoplankton variables (i.e., F_L, PP_{eu} and chl *a*) at least in the study area.

BGD
12, 12611–12651, 2015

4.2 Timing of the MIZ bloom

We have shown that the timing of the MIZ bloom occurrence is tightly coupled with the TSR except for the western side of the Bering Strait and coastal Alaska. Consistent with Perrette et al. (2011), CMAX generally occurs within ~ 20 days after sea ice melt (Fig. 3c). Some past studies have discussed the relationship between the timing of the bloom and sea ice melt (e.g., Hunt et al., 2002, 2011; Kahru et al., 2010; Perrette et al., 2010). Sigler et al. (2014) have evaluated that earlier sea ice retreat (earlier than mid-March) cannot trigger ice-related phytoplankton blooms, because there is insufficient light to support primary production due to a well-mixed water column in the southern Bering Sea (Hunt et al., 2002). In such years, the spring bloom occurs in late spring (May or early June). In contrast, the bloom occurrs immediately after sea ice melt in the late ice retreat years when it occurs later than mid-March. Brown and Arrigo (2013) evaluated the relationship between the timing of sea ice retreat and spring phytoplankton blooms using satellite remote sensing data, and showed that the relationship described above is applicable in the southern but not in the northern Bering Sea. Since our analyses were conducted on more northward centered regions than in the studies of Hunt et al. (2002, 2011), our results revealed that timing of CMAX generally followed TSR, and that was consistent with reportef in previous studies (Kahru et al., 2011; Perrette et al., 2011; Brown and Arrigo, 2013 and Ji et al., 2013). However, our results also indicate that CMAX date is delayed in the Bering Strait and along the coast of Alaska (Fig. 3c). This suggests that the timing of the annual maximum phytoplankton biomass does not fully depend on the sea ice retreat timing and the subsequent nutrient conditions, because there are large amounts of nutrients even in summer in the Bering Strait, due to inflow of nutrient-rich Anadyr Water (Springer and McRoy, 1993; Springer et al., 1996). Optical contamination of CDOM in chl *a* retrieval can also affect the values of CMAX especially in the area where the Alaskan Coastal Water (ACW) flows. Matsuoka et al. (2011) suggested that the ACW contributes to the high value of CDOM absorption ($a_y(\lambda)$), which can cause overestimation of satellite chl *a*, because

BGD
12, 12611–12651, 2015

CDOM absorbs light at some of the same wavelengths as chl *a* (Matsuoka et al., 2007; Naik et al., 2013). Accordingly, CMAX in the ACW, especially in Kotzebue and Norton Sounds, should be carefully treated, because chl *a* in this area might contain large uncertainty.

Our results revealed that the spring open water bloom generally occurs during the MIZ bloom period at least in our study area (hereafter referred to as the MIZ bloom). The MIZ bloom can affect growth and reproduction of grazers because they greatly depend on the bloom for energy (e.g., Hunt et al., 2002, 2011). While bloom timing is important for juvenile stages of zooplankton, the phytoplankton community size composition and its relationship to the yearly change of sea ice retreat timing is also crucial to understand zooplankton reproduction and development (Leu et al., 2011).

4.3 Influence of TSR on phytoplankton size composion during the MIZ blooms

Spatial analysis using continuous ocean color data from SeaWiFS to MODIS-Aqua observations revealed phytoplankton community size structure during the MIZ bloom responds to yearly change of TSR. Our results indicate that large phytoplankton tend to increase and/or can maintain their high biomass proportion in early ice retreat years, and vice versa (Fig. 4a). The relationships between SST and TSR, and between ΔOHC and TSR suggest that the development of the surface mixed layer is related to changes in TSR. Unfortunately, salinity stratification is difficult to infer using satellite or re-analysis data. However, Alexander and Niebauer, (1981) showed the development of both salinity and thermal stratification induces water column stability, which generally triggers the ice-edge phytoplankton bloom in the Bering Sea. Thus, ΔOHC was used as a proxy of development of the surface mixed layer. Since sea ice retreat occurs before summer solstice even in the late ice retreat years on the shelf (Fig. 3a), thermal stratification is likely to be delayed due to weak solar radiation and low air temperature in early ice retreat years. In contrast, stronger solar radiation with warmer air temperature can lead to faster stratification during the MIZ bloom period in late ice retreat years. Hence, higher surface nutrient concentrations are expected in early ice retreat

BGD
12, 12611–12651, 2015

years, and conversely, nutrients can immediately be consumed by large phytoplankton in late ice retreat years.

In addition, under-ice phytoplankton or ice-algal blooms can also be controlling factors for the relationship between F_L and TSR. Arrigo et al. (2012) discovered that phytoplankton blooms can occur even in under-ice water columns where sufficient light for phytoplankton growth penetrates into the water due to thin ice or presence of meltponds. Lowry et al. (2014) suggested that under ice phytoplankton blooms could frequently and widely occur on the Chukchi Sea shelf, where negative ρ between TSR and F_L was found in the current study. Since thin first-year ice dominates in the shelf areas of the Chukchi and Bering Seas (Comiso et al., 2008), sufficient light can penetrate into the water column when solar radiation is strong enough. We noted that sea ice retreats before summer solstice (i.e., before the yearly maximum of solar radiation occurs). Accordingly, the light levels of the under-ice water column would be better for phytoplankton growth in late ice retreat years, and under-ice phytoplankton blooms may utilize nutrients in the surface layer before sea ice retreats. As a result, the large phytoplankton taxa during the MIZ blooms cannot retain their dominance long in years with the late ice retreat, since as surface nutrients become depleted, smaller phytoplankton taxa are favored.

However, these scenarios are not the case for the western side of Bering Strait (2 % of the study area), where the correlation between F_L and timing of sea ice retreat showed a positive significant relationship (Fig. 4a) (Table 2). It is notable that this is the same area where CMAX date does not follow the date of sea ice retreat (Fig. 3c). This analysis revealed that late sea ice retreat does not limit phytoplankton growth during post-bloom conditions in this area. One possible scenario is that the major limiting factor for phytoplankton growth is water temperature rather than light and nutrient availability. Bering Strait is known as a nutrient-rich region even in summer (Springer and McRoy, 1993), and there is sufficient light. Another scenario is that higher nutrient consumption in upstream regions can reduce horizontal advection of nutrients into the Bering Strait in early ice retreat years, and vice versa.

BGD
12, 12611–12651, 2015

Based on the spatial statistical analysis, we suggest a general relationship between yearly change of phytoplankton community size structure and timing of sea ice retreat during the MIZ bloom period. It has been reported that sea ice retreat timing can alter seasonal succession of phytoplankton in Svalbard (Leu et al., 2011) and the northern Chukchi Sea (Fujiwara et al., 2014). Our results also suggest that phytoplankton cell size composition can change with timing of sea ice retreat in the shelf region of Bering and Chukchi Seas during the MIZ bloom. These results provide important information to help understand food quality for organisms that depend on the MIZ blooms as an energy source. However, it should be noted that the relationships between TSR and phytoplankton size might not be applicable to the entire Arctic, because our focused region is characterized by shallow bathymetry, sea ice retreat near summer solstice (Fig. 3a), and dominance of thin first year ice. These unique environmental characteristics can tightly couple phytoplankton bloom and sea ice dynamics.

4.4 Factors controlling annual net primary production

Previous studies have reported that variability of annual primary production in the Arctic Ocean largely depends on the length of the open water period and open water area, which contribute to length of growing season and growing area, respectively (Arrigo et al., 2008, 2011; and Pabi et al., 2008). Similar relationship was also reported for the Bering Sea where sea ice covers seasonally (Brown et al., 2012). On the other hand, Trembley and Gagnon (2009) showed that cumulative irradiance during the growth season is not always a primary driver of APP in the Arctic. The initial concentration of nitrate at the onset of growth season is rather important in the high Arctic Ocean (Trembley and Gagnon, 2009). However, nitrate concentration uniformly reaches 10–20 µM at the onset of growth season even in the surface water due to strong vertical mixing both in the Chukchi and Bering shelves (e.g., Sambrotto et al., 1986; Codispoti et al., 2005), which is enough to support large open water and/or under-ice bloom. Due to this, our findings suggest that the length of open water period plays a significant role in controlling APP in the study region, especially in the northern Chukchi shelf (Fig. 5a).

BGD
12, 12611–12651, 2015

Nevertheless, the contribution of the length of open water period to APP was relatively smaller in the Bering Sea. In contrast, the contribution of F_L to APP is larger than the open water period in the Bering and central Chukchi Sea shelves (Fig. 5b). This is because, while the range of inter-annual variation of open water period for both shelf regions is similar (1–2 months), it accounts for up to ~ 35 % of mean growth season on the Chukchi shelf (~ 6 months), which is significantly larger than that of in the Bering shelf (up to ~ 20 %). It is likely that dominance of highly productive large phytoplankton (i.e., diatoms) greatly affect variability of APP in regions where the open water period is relatively longer. Therefore, some controlling factors for phytoplankton size structure, such as nutrient supply or grazing, are suggested to be important to determine APP in the southern shelf region. In fact, Eisner et al. (2015) reported wind-induced mixing during late summer to fall positively affect chl *a* and proportion of larger-size phytoplankton in less ice extent years in the southern Bering Sea. In contrast, a positive but relatively small contribution of SST to APP also dominated in the shelf region; its magnitude was relatively lower than the other two factors. The positive contribution of warmer temperature to APP was reported in Mueter et al. (2009) and Brown et al. (2011, 2013) in the Bering Sea. Temperature can positively and directly affect the photosynthetic activity of phytoplankton (Eppley et al., 1972) or temperature was an indirect effect of early sea ice retreat. Nevertheless, other controlling factors would be more important in high latitude regions because of small seasonal variability of SST compared to mid-latitude seas. In particular, SST contributed rather negatively to APP along the shelf break of the Bering Sea (Fig. 5c), where the partial regression coefficient of F_L was positive (Fig. 5b). This may be because colder SST during the MIZ bloom period promotes larger F_L with high productivity (discussed in Sect. 4.2). Since the Arctic Ocean is predicted to be more ice-free ocean by many models (Perovich and Richter-Menge, 2009), it is suggested that the contiribution of phytoplankton size composition to APP will be larger in the future. Therefore, understanding the relationship between the timing of sea ice retreat and phytoplankton community composition during

BGD
12, 12611–12651, 2015

the bloom period might advance the knowledge of biogeochemical cycles and energy transfer to higher trophic level organisms in this area.

5 Conclusions

To the best of our knowledge, this is the first study that captures the relationship between phytoplankton size structure and sea ice dynamics using satellite remote sensing data. Although satellite remote sensing data contains large observation error compared to in situ measurements, it is a powerful tool to determine the spatial variability of the response of primary producers to environmental change. In addition, the continuous observation period for ocean color remote sensing currently exceeds 17 years over the term of several sensors (e.g., SeaWiFS, MODIS and MERIS). Spatio-temporal statistical analysis using long time series of ocean color data can quantify the response of phytoplankton communities to environmental change, and such statistical generalization is important to predict future ecosystem responses or conduct risk assessments.

To conclude, this study reveals that the timing of sea ice retreat can alter phytoplankton size composition during the MIZ bloom period. That is, earlier sea ice retreat is linked with larger proportions of large phytoplankton taxa in colder water during cold MIZ bloom periods, and vice versa, in the shelf regions of the Bering and Chukchi Seas. Our findings can potentially be linked with ecosystem changes reported in this region (Grebmeier et al., 2012 and references) considering the bottom-up energy transfer process via food web and predator-prey body size relationships. It has been reported that algal grazers greatly depend on the spring bloom as their energy source. For example, timing of the spring bloom, sea ice and temperature significantly affects the recruitment of copepods in the Bering Sea (Hunt et al., 2002, 2011). Food quality during the spring bloom, which varies with species composition, also has a significant effect on secondary production (Søreide et al., 2010; Leu et al., 2011). Thus, comprehension of the relationships between sea ice dynamics, phytoplankton community structure and envi-

BGD
12, 12611–12651, 2015

ronmental conditions are important for assessing the production, activity or recruitment of higher trophic level organisms in the northern Bering and Chukchi Seas.

Appendix A

There are slight differences in observation band between SeaWiFS and MODIS; MODIS measures $R_{rs}(488)$ and $R_{rs}(667)$ while SeaWiFS measures $R_{rs}(490)$ and $R_{rs}(670)$. $R_{rs}(\lambda)$ values between them also differ even though they were obtained in same day and same location due to some uncertainties (i.e., atmospheric correction, sensor sensitivity, zenith angle). Therefore, bias correction between them was conducted before analyzing and processing the continuous time series data. We calculated bias and RMSE between SeaWiFS-$R_{rs}(\lambda)$ and MODIS-$R_{rs}(\lambda)$ (λ = 412, 443, 490, 555 and 667 nm) changing the correction factor from 0.5 to 1.5 to linearly convert SeaWiFS-$R_{rs}(\lambda)$ into MODIS-$R_{rs}(\lambda)$ (Fig. A1). The bias and RMSE calculation was conducted using Level-3 daily 9 km matched-up pixels from 2003 to 2007. Then, optimum correction factors for each band were determined to remove the biases (listed in Table A1). To evaluate the effect of the conversion, we calculated the biases of ocean color products (i.e., F_L, chl *a* and $a_{ph}(443)$) between MODIS and default SeaWiFS, and converted SeaWiFS using daily matched-up images during 2003–2007 for the study area. Frequency of the biases and their statistics are shown in Fig. A2a–c. Every product were underestimated by default SeaWiFS relative to MODIS, though the biases were almost completely removed after the SeaWiFS-$R_{rs}(\lambda)$ conversion. Then, simple averaging between SeaWiFS and MODIS products was conducted for overlapped observation periods to merge them and increase the number of observation points.

Appendix B

A large number of $a_{ph}(\lambda)$ values were underestimated using default QAA (Lee et al., 2002, 2009), especially in longer λ (i.e., $\lambda > 490$ nm). This is probably due to the uncer-

BGD
12, 12611–12651, 2015

tainty and error contained in the analytical and empirical equations for deriving $a_{ph}(\lambda)$. We attempted to overcome this problem by tuning the calculation step of QAA. QAA retrieves $a_{ph}(\lambda)$ by subtracting the absorption coefficient of detritus + CDOM ($a_{dg}(\lambda)$) and pure sea water ($a_w(\lambda)$) from the total absorption coefficient($a_t(\lambda)$):

$$a_{ph}(\lambda) = a_t(\lambda) - a_{dg}(\lambda) - a_w(\lambda), \quad \text{(B1)}$$

and

$$a_{dg}(\lambda) = a_{dg}(443)\exp[-S_{dg}(\lambda - 443)], \quad \text{(B2)}$$

where S_{dg} is spectral slope of $a_{dg}(\lambda)$, and it is derived as,

$$S_{dg} = S_{init} + \frac{0.002}{0.6 + r_{rs}(443)/r_{rs}(555)}, \quad \text{(B3)}$$

where $S_{init} = 0.015$ for the default QAA. The underestimation of $a_{ph}(\lambda)$ is due to over-subtracting $a_t(\lambda)$ with $a_{dg}(\lambda)$ and $a_w(\lambda)$. That is, during derivation of $a_{ph}(\lambda)$, the default retrieval of $a_{dg}(\lambda)$ was overestimated. To avoid such underestimation of $a_{ph}(\lambda)$, we conducted tuning of QAA determining optimum S_{init} for the study area. Optimization was performed using in situ collected $R_{rs}(\lambda)$ and $a_{ph}(\lambda)$. In situ data was obtained from the five cruises of R/V *Mirai* (Shimada, 2008; Kikuchi, 2009, 2012; Itoh, 2010; Nishino, 2013) and three cruises of TR/V *Oshoro-maru* conducted in the Bering and Chukchi Seas from 2007–2013 ($N = 220$). We computed RMSE between in situ and modeled $a_{ph}(\lambda)$ changing S_{init} from 0.01 to 0.03 with 0.0005 increments (Fig. B1). Then optimum S_{init} was determined as the value that minimized the average RMSE (= 0.019).

Acknowledgements. We are grateful to the captain and crews of TR/S *Oshoro-maru* (Hokkaido University), R/V *Mirai* (JAMSTEC), R/V *Dyson* (NOAA, NMFS) and F/V *Sea Storm* for their kind support during our observations. We also thank the staff of Global Ocean Development, Inc and Marine Works Japan, Ltd. for their skillful work aboard the ship and for data analysis.

BGD
12, 12611–12651, 2015

We also thank A. Matsuoka for his valuable suggestions. Satellite data were provided by Goddard Space Flight Center (GSFC, NASA), Physical Oceanography Distributed Active Archive Center (PODAAC, NASA), and National Snow and Ice Data Center (NSIDC) at the University of Colorado. This study was funded by GRENE Arctic Climate Change Research Project and GCOM-C mission by JAXA.

References

Alexander, V. and Niebaueer, H.: Oceanography of the eastern Bering Sea ice-edge zone in spring, Limnol. Oceanogr., 26, 1111–1125, 1981.

Alvain, S., Moulin, C., Dandonneau, Y., and Bréon, F.: Remote sensing of phytoplankton groups in case 1 waters from global SeaWiFS imagery, Deep-Sea Res. Part I, 52, 1989–2004, 2005.

Ardyna, M., Babin, M., Gosselin, M., Devred, E., Bélanger, S., Matsuoka, A., and Tremblay, J.-É.: Parameterization of vertical chlorophyll *a* in the Arctic Ocean: impact of the subsurface chlorophyll maximum on regional, seasonal, and annual primary production estimates, Biogeosciences, 10, 4383–4404, doi:10.5194/bg-10-4383-2013, 2013.

Arrigo, K. R. and Van Dijken, G. L.: Secular trends in Arctic Ocean net primary production, J. Geophys. Res., 116, doi:10.1029/2011JC007151, 2011.

Arrigo, K. R., Van Dijken, G., and Pabi, S.: Impact of a shrinking Arctic ice cover on marine primary production, Geophys. Res. Lett., 35, L19603, doi:10.1029/2008GL035028, 2008.

Arrigo, K. R., Perovich, D. K., Pickart, R. S., Brown, Z. W., Van Dijken, G. L., Lowry, K. E., Mills, M. M., Palmer, M. A., Balch, W. M., Bahr, F., Bates, N. R., Benitez-Nelson, C., Bowler, B., Brownlee, E., Ehn, J. K., Frey, K. E., Garley, R., Laney, S. R., Lubelczyk, L., Mathis, J., Matsuoka, A., Mitchell, B. G., Moore, G. W. K., Ortega-Retuerta, E., Pal, S., Polashenski, C. M., Reynolds, R. A., Schieber, B., Sosik, H. M., Stephens, M., and Swift, J. H.: Massive phytoplankton blooms under Arctic Sea ice, Science, 336, 1408–1408, 2012.

Behrenfeld, M. J. and Falkowski, P. G.: Photosynthetic rates derived from satellite-based chlorophyll concentration, Limnol. Oceanogr., 42, 1–20, 1997.

Brewin, R. J. W., Sathyendranath, S., Hirata, T., Lavender, S. J., Barciela, R. M., and Hardman-Mountford, N. J.: A three-component model of phytoplankton size class for the Atlantic Ocean, Ecol. Model., 221, 1472–1483, doi:10.1016/j.ecolmodel.2010.02.014, 2010.

Brock, T. D.: Calculating solar radiation for ecological studies, Ecol. Model., 14, 1–19, 1981.

BGD
12, 12611–12651, 2015

Brown, Z. W. and Arrigo, K. R.: Sea ice impacts on spring bloom dynamics and net primary production in the Eastern Bering Sea, J. Geophys. Res.-Oceans, 118, 43–62, doi:10.1029/2012JC008034, 2013.

Brown, Z. W., Van Dijken, G. L., and Arrigo, K. R.: A reassessment of primary production and environmental change in the Bering Sea, J. Geophys. Res.-Oceans, 116, C08014, doi:10.1029/2010JC006766, 2011.

Brown, Z. W., Lowry, K. E., Palmer, M. A., Van Dijken, G. L., Mills, M. M., Pickart, R. S., and Arrigo, K. R.: Characterizing the subsurface chlorophyll a maximum in the Chukchi Sea and Canada Basin, Deep-Sea Res. Part II, doi:10.1016/j.dsr2.2015.02.010, in press, 2015.

Ciotti, A. and Bricaud, A.: Retrievals of a size parameter for phytoplankton and spectral light absorption by colored detrital matter from water-leaving radiances at SeaWiFS channels in a continental shelf region off Brazil, Limnol. Oceanogr.-Meth., 4, 237–253, 2006.

Codispoti, L. A., Flagg, C., Kelly, V., and Swift, J. H.: Hydrographic conditions during the 2002 SBI process experiments, Deep-Sea Res. Part II, 52, 3199–3226, doi:10.1016/j.dsr2.2005.10.007, 2005.

Comiso, J. C., Parkinson, C. L., Gersten, R., and Stock, L.: Accelerated decline in the Arctic Sea ice cover, Geophys. Res. Lett., 35, L01703, doi:10.1029/2007GL031972, 2008.

Cota, G., Wang, J., and Comiso, J.: Transformation of global satellite chlorophyll retrievals with a regionally tuned algorithm, Remote Sens. Environ., 90, 373–377, 2004.

Coyle, K. O., Pinchuk, A. I., Eisner, L. B., and Napp, J. M.: Zooplankton species composition, abundance and biomass on the eastern Bering Sea shelf during summer: the potential role of water-column stability and nutrients in structuring the zooplankton community, Deep-Sea Res. Part II, 55, 1775–1791, doi:10.1016/j.dsr2.2008.04.029, 2008.

Devred, E., Sathyendranath, S., Stuart, V., and Platt, T.: A three component classification of phytoplankton absorption spectra: application to ocean-color data, Remote Sens. Environ., 115, 2255–2266, doi:10.1016/j.rse.2011.04.025, 2011.

Eisner, L. B., Gann, J. C., Ladd, C., Cieciel, K., and Mordy, C. W.: Late summer early fall phytoplankton biomass (chlorophyll *a*) in the eastern Bering Sea: spatial and temporal variations and factors afecting chlorophyll a concentrations, Deep-Sea Res. Pt. II, doi:10.1016/j.dsr2.2015.07.012, 2015.

Eppley, R. W.: Temperature and phytoplankton growth in the sea, Fish. B-NOAA, 70, 1063–1085, 1972.

BGD
12, 12611–12651, 2015

Fujiwara, A., Hirawake, T., Suzuki, K., and Saitoh, S.-I.: Remote sensing of size structure of phytoplankton communities using optical properties of the Chukchi and Bering Sea shelf region, Biogeosciences, 8, 3567–3580, doi:10.5194/bg-8-3567-2011, 2011.

Fujiwara, A., Hirawake, T., Suzuki, K., Imai, I., and Saitoh, S.-I.: Timing of sea ice retreat can alter phytoplankton community structure in the western Arctic Ocean, Biogeosciences, 11, 1705–1716, doi:10.5194/bg-11-1705-2014, 2014.

Grebmeier, J. M.: Shifting Patterns of Life in the Pacific Arctic and Sub-Arctic Seas, Annu. Rev. Mar. Sci., 4, 63–78, doi:10.1146/annurev-marine-120710-100926, 2012.

Grebmeier, J. M. and Dunton, K.: Benthic processes in the northern Bering/Chukchi seas: status and global change, in: Impacts of changes in sea ice and other environmental parameters in the Arctic, edited by: Huntington, H. P., Report of the Marine Mammal Commission Workshop, Girdwood, Alaska, 61–71, 2000.

Grebmeier, J. M., McRoy, C., and Feder, H.: Pelagic-benthic coupling on the shelf of the northern Bering and Chukchi seas. 1. Food supply source and benthic biomass, Mar. Ecol.-Prog. Ser., 48, 57–67, 1988.

Grebmeier, J. M., Cooper, L. W., Feder, H. M., Sirenko, B. I., Ecosystem Dynamics of the Pacific-Influenced Northern Bering and Chukchi Seas, Prog. Oceanogr., 71, 331–361, 2006a.

Grebmeier, J. M., Overland, J. E., Moore, S. E., Farley, E. V., Carmack, E. C., Cooper, L. W., Frey, K. E., Helle, J. H., McLaughlin, F. A., and McNutt, S. L.: A major ecosystem shift in the northern Bering Sea, Science, 311, 1461–1464, 2006b.

Grebmeier, J. M., Moore, S., and Overland, J.: Biological response to recent Pacific Arctic Sea ice retreats, EOS Trans., 91, 161–162, 2010.

Hill, V., Cota, G., and Stockwell, D.: Spring and summer phytoplankton communities in the Chukchi and eastern Beaufort Seas, Deep-Sea Res. Part II, 52, 3369–3385, 2005.

Hill, V. J., Matrai, P. A., Olson, E., Suttles, S., Steele, M., Codispoti, L. A., and Zimmerman, R. C.: Synthesis of integrated primary production in the Arctic Ocean: I I. In situ and remotely sensed estimates, Prog. Oceanogr., 110, 107–125, 2013.

Hirata, T., Hardman-Mountford, N. J., Brewin, R. J. W., Aiken, J., Barlow, R., Suzuki, K., Isada, T., Howell, E., Hashioka, T., Noguchi-Aita, M., and Yamanaka, Y.: Synoptic relationships between surface Chlorophyll-*a* and diagnostic pigments specific to phytoplankton functional types, Biogeosciences, 8, 311–327, doi:10.5194/bg-8-311-2011, 2011.

Hirata, T., Saux-Picart, S., Hashioka, T., Aita-Noguchi, M., Sumata, H., Shigemitsu, M., Allen, J. I., and Yamanaka, Y.: A comparison between phytoplankton community structures

BGD
12, 12611–12651, 2015

derived from a global 3-D ecosystem model and satellite observation, J. Marine Syst., 109–110, 129–137, doi:10.1016/j.jmarsys.2012.01.009, 2013.
Hirawake, T., Takao, S., Horimoto, N., Ishimaru, T., Yamaguchi, Y., and Fukuchi, M.: A phytoplankton absorption-based primary productivity model for remote sensing in the Southern Ocean, Polar Biol., 34, 291–302, doi:10.1007/s00300-010-0949-y, 2011.
Hirawake, T., Shinmyo, K., Fujiwara, A., and Saitoh, S.-I.: Satellite remote sensing of primary productivity in the Bering and Chukchi Seas using an absorption-based approach, ICES J. Mar. Sci., 69, 1194–1204, 2012.
Hunt Jr., G. L., Stabeno, P., Walters, G., Sinclair, E., Brodeur, R. D., Napp, J. M., and Bond, N. A.: Climate change and control of the southeastern Bering Sea pelagic ecosystem, Deep-Sea Res. Part II, 49, 5821–5853, 2002.
Hunt Jr., G. L., Coyle, K. O., Eisner, L. B., Farley, E. V., Heintz, R. A., Mueter, F., Napp, J. M., Overland, J. E., Ressler, P. H., Salo, S., and Stabeno, P. J.: Climate impacts on eastern Bering Sea foodwebs: a synthesis of new data and an assessment of the Oscillating Control Hypothesis, ICES J. Mar. Sci., 68, 1230–1243, doi:10.1093/icesjms/fsr036, 2011.
Huntley, M. E. and Lopez, M.: Temperature-dependent production of marine copepods: a global synthesis, Am. Nat., 140, 201–242, doi:10.1086/285410, 1992.
Itoh, M.: R/V *Mirai* Cruise Report MR10-05. Yokosuka: JAMSTEC, 2010.
Ji, R., Jin, M., and Varpe, Ø.: Sea ice phenology and timing of primary production pulses ub the Arctic Ocean, Glob. Change Biol., 19, 734–741, doi:10.1111/gcb.12074, 2013.
Kahru, M., Brotas, V., Manzano-Sarabia, M., and Mitchell, B. G.: Are phytoplankton blooms occurring earlier in the Arctic?, Glob. Change Biol., 17, 1733–1739, doi:10.1111/j.1365-2486.2010.02312.x, 2011.
Kalnay, E., Kanamitsu, M., Kistler, R., Collins, W., Deaven, D., Gandin, L., Iredell, M., Saha, S., White, G., Woollen, J., Zhu, Y., Leetmaa, A., Reynolds, R., Chelliah, M., Ebisuzaki, W., Higgins, W., Janowiak, J., Mo, K. C., Ropelewski, C., Wang, J., Jenne, R., and Joseph, D.: The NCEP/NCAR 40-Year Reanalysis Project, B. Am. Meteorol. Soc., 77, 437–471, doi:10.1175/1520-0477(1996)077<0437:TNYRP>2.0.CO;2, 1996.
Kikuchi, T.: R/V *Mirai* Cruise Report MR09-03. Yokosuka: JAMSTEC, 2009.
Kikuchi, T.: R/V *Mirai* Cruise Report MR12-E03. Yokosuka: JAMSTEC, 2012.
Kostadinov, T. S., Siegel, D. A., and Maritorena, S.: Retrieval of the particle size distribution from satellite ocean color observations, J. Geophys. Res., 114, C09015, doi:10.1029/2009JC005303, 2009.

BGD
12, 12611–12651, 2015

Lee, Z., Carder, K., and Arnone, R.: Deriving inherent optical properties from water color: a multiband quasi-analytical algorithm for optically deep waters, Appl. Optics, 41, 5755–5772, 2002.
Lee, Z., Weidemann, A., Kindle, J., Arnone, R., Carder, K., and Davis, C.: Euphotic zone depth: its derivation and implication to ocean-color remote sensing, J. Geophys. Res., 112, C03009, 2007.
Lee, Z., Lubac, B., Werdell, J., and Arnone, R.: An Update of the Quasi-Analytical Algorithm (QAA_v5), http://www.ioccg.org/groups/Software_OCA/QAA_v5.pdf, 1–9, available at: http://www.ioccg.org/groups/software.html (last access: 28 March 2011), 2009.
Lowry, K. E., Van Dijken, G. L., and Arrigo, K. R.: Evidence of under-ice phytoplankton bloom in the Chukchi Sea from 1998–2012, Deep-Sea Res. Part II, 105, 105–117, doi:10.1016/j.dsr2.2014.03.013, 2014.
Markus, T. and Cavalieri, D. J.: An enhancement of the NASA Team sea ice algorithm, IEEE T. Geosci. Remote, 38, 1387–1398, doi:10.1109/36.843033, 2000.
Matsuoka, A., Huot, Y., Shimada, K., Saitoh, S.-I., and Babin, M.: Bio-optical characteristics of the western Arctic Ocean: implications for ocean color algorithms, Can. J. Remote Sens., 33, 503–518, doi:10.5589/m07-059, 2007.
Matsuoka, A., Hill, V., Huot, Y., Babin, M., and Bricaud, A.: Seasonal variability in the light absorption properties of western Arctic waters: Parameterization of the individual components of absorption for ocean color applications, J. Geophys. Res., 116, C02007, doi:10.1029/2009JC005594, 2011.
Mizobata, K. and Shimada, K.: East–west asymmetry in surface mixed layer and ocean heat content in the Pacific sector of the Arctic Ocean derived from AMSR-E sea surface temperature, Deep-Sea Res. Part II, 77–80, 62–69, doi:10.1016/j.dsr2.2012.04.005, 2012.
Moore, S. E., Grebmeier, J. M., and Davies, J. R.: Gray whale distribution relative to forage habitat in the northern Bering Sea: current conditions and retrospective summary, Can. J. Zool., 81, 734–742, doi:10.1139/z03-043, 2003.
Mouw, C. B. and Yoder, J. A.: Optical determination of phytoplankton size composition from global SeaWiFS imagery, J. Geophys. Res., 115, C12018, doi:10.1029/2010JC006337, 2010.
Mueter, F. J., Broms, C., Drinkwater, K. F., Friedland, K. D., Hare, J. A., Hunt Jr., G. L., Melle, W., and Taylor, M.: Ecosystem responses to recent oceanographic variabil-

BGD
12, 12611–12651, 2015

ity in high-latitude Northern Hemisphere ecosystems, Prog. Oceanogr., 81, 93–110, doi:10.1016/j.pocean.2009.04.018, 2009.
Naik, P., D'Sa, E. J., Gomes, H. D. R., Goés, J. I., and Mouw, C. B.: Light absorption properties of southeastern Bering Sea waters: analysis, parameterization and implications for remote sensing, Remote Sens. Environ., 134, 120–134, 2013.
Niebauer, J. H.: Bio-physical oceanographic interactions at the edge of the Arctic ice pack, J. Marine Syst., 2, 209–232, doi:10.1016/0924-7963(91)90025-P, 1991.
Nishino, S.: R/V *Mirai* Cruise Report MR13-06. Yokosuka: JAMSTEC, 2013.
Pabi, S., Van Dijken, G. L., and Arrigo, K. R.: Primary production in the Arctic Ocean, 1998–2006, J. Geophys. Res., 113, C08005, doi:10.1029/2007JC004578, 2008.
Parsons, T. R., Maita, A., and Lalli, C. M.: Fluorometric determination of chlorophylls, in: A Manual of Chemical & Biological Methods for Seawater Analysis, Pergamon, Amsterdam, 107–109, 1984.
Perovich, D. K. and Richter-Menge, J. A.: Loss of sea ice in the Arctic, Annu. Rev. Mar. Sci., 1, 417–441, doi:10.1146/annurev.marine.010908.163805, 2009.
Perrette, M., Yool, A., Quartly, G. D., and Popova, E. E.: Near-ubiquity of ice-edge blooms in the Arctic, Biogeosciences, 8, 515–524, doi:10.5194/bg-8-515-2011, 2011.
Piepenburg, D.: Recent research on Arctic benthos: common notions need to be revised, Polar Biol., 28, 733–755, 2005.
Sambrotto, R. N., Niebauer, H. J., Goering, J. J., and Iverson, R. L.: Relationships among vertical mixing, nitrate uptake, and phytoplankton growth during the spring bloom in the southeast Bering Sea middle shelf, Cont. Shelf Res., 5, 161–198, doi:10.1016/0278-4343(86)90014-2, 1986.
Sambrotto, R. N., Mordy, C., Zeeman, S. I., Stabeno, P. J., and Macklin, S. A.: Physical forcing and nutrient conditions associated with patterns of Chl *a* and phytoplankton productivity in the southeastern Bering Sea during summer, Deep-Sea Res. Part II, 55, 1745–1760, doi:10.1016/j.dsr2.2008.03.003, 2008.
Sathyendranath, S., Watts, L., Devred, E., Platt, T., Caverhill, C., and Maass, H.: Discrimination of diatoms from other phytoplankton using ocean-colour data, Mar. Ecol.-Prog. Ser., 272, 59–68, 2004.
Sheffield, G., Fay, F. H., Feder, H., and Kelly, B. P.: Laboratory digestion of prey and interpretation of walrus stomach contents, Mar. Mammal Sci., 17, 310–330, doi:10.1111/j.1748-7692.2001.tb01273.x, 2001.

BGD
12, 12611–12651, 2015

Shimada, K.: R/V *Mirai* Cruise Report MR08-04. Yokosuka: JAMSTEC, 2008.
Sigler, M. F., Stabeno, P. J., Eisner, L. B., Napp, J. M., and Mueter, F. J.: Spring and fall phytoplankton blooms in a productive subarctic ecosystem, the eastern Bering Sea, during 1995–2011, Deep-Sea Res. Part II, 109, 71–83, doi:10.1016/j.dsr2.2013.12.007, 2014.
Springer, A. M. and McRoy, C. P.: The paradox of pelagic food webs in the northern Bering Sea – III. Patterns of primary production, Cont. Shelf Res., 13, 575–599, doi:10.1016/0278-4343(93)90095-F, 1993.
Springer, A. M., McRoy, C. P., and Flint, M. V.: The Bering Sea Green Belt: shelf-edge processes and ecosystem production, Fish. Oceanogr., 5, 205–223, 1996.
Søreide, J. E., Leu, E., Berge, J., Graeve, M., and Falk-Petersen, S.: Timing of blooms, algal food quality and *Calanus glacialis* reproduction and growth in a changing Arctic, Glob. Change Biol., 16, 3154–3163, doi:10.1111/j.1365-2486.2010.02175.x, 2010.
Takao, S., Hirawake, T., Wright, S. W., and Suzuki, K.: Variations of net primary productivity and phytoplankton community composition in the Indian sector of the Southern Ocean as estimated from ocean color remote sensing data, Biogeosciences, 9, 3875–3890, doi:10.5194/bg-9-3875-2012, 2012.
Trembley, J.-E. and Gagnon, J.: The effect of irradiance and nutrient supply on the productivity of Arctic waters: a perspective on climate change, in: Influence of Climate Change on the Changing Arctic and Sub-Arctic Conditions, edited by: Nihoul, J. C. J. and Kostianoy, A. G., Springer, Netherlands, 73–93, 2009.
Uitz, J., Claustre, H., Morel, A., and Hooker, S. B.: Vertical distribution of phytoplankton communities in open ocean: an assessment based on surface chlorophyll, J. Geophys. Res., 111, C08005, doi:10.1029/2005JC003207, 2006.
Welschmeyer, N.: Fluorometric analysis of chlorophyll *a* in the presence of chlorophyll *b* and pheopigments, Limnol. Oceanogr., 39, 1985–1992, 1994.

BGD
12, 12611–12651, 2015

Table 1. List of symbol and units.

abbreviations	definitions	unit
a_{ph}	absorption coefficient of phytoplankton	m^{-1}
chl *a*	chlorophyll *a* concentration	$mg\,m^{-3}$
APP	annual net primary production	$mg\,C\,m^{-2}\,yr^{-1}$
CMAX	annual maximum value of chl *a*	$mg\,m^{-3}$
F_L	index of phytoplankton size composition	% chl *a*
MIZ	marginal ice zone	
PAR	photosynthetically available radiation	$Einstein m^{-2}\,day^{-1}$
PP_{eu}	euphotic-depth integrated primary production	$mg\,C\,m^{-2}\,day^{-1}$
R_{rs}	remote sensing reflectance	sr^{-1}
SST	sea surface temperature	°C
TSR	timing of sea ice retreat	day of year
Z_{eu}	euphotic depth	mg
ΔOHC	changes of ocean heat contents during bloom period	J

BGD
12, 12611–12651, 2015

Table 2. Area proportions of Spearman's rank correlation coefficient ρ between timing of sea ice retreat and F_L, SST, ΔOHC and PAR, in the study region are shown. Their spatial distribution are also shown in Fig. 4a–d.

	positive ρ			negative ρ		
	**	*		**	*	
F_L and TSR	2 %	4 %	32 %	15 %	22 %	68 %
SST and TSR	65 %	71 %	92 %	1 %	1 %	8 %
ΔOHC and TSR	3 %	5 %	13 %	61 %	68 %	87 %
PAR and TSR	27 %	35 %	66 %	12 %	15 %	34 %

** and * denote $p < 0.05$ and $p < 0.1$, respectively.

BGD
12, 12611–12651, 2015

Table A1. Correction factors to convert SeaWiFS-$R_{rs}(\lambda)$ into MODIS-$R_{rs}(\lambda)$.

λ	correction factor
412	1.04
443	0.99
488	1.00
555	0.94
667	0.92

BGD
12, 12611–12651, 2015

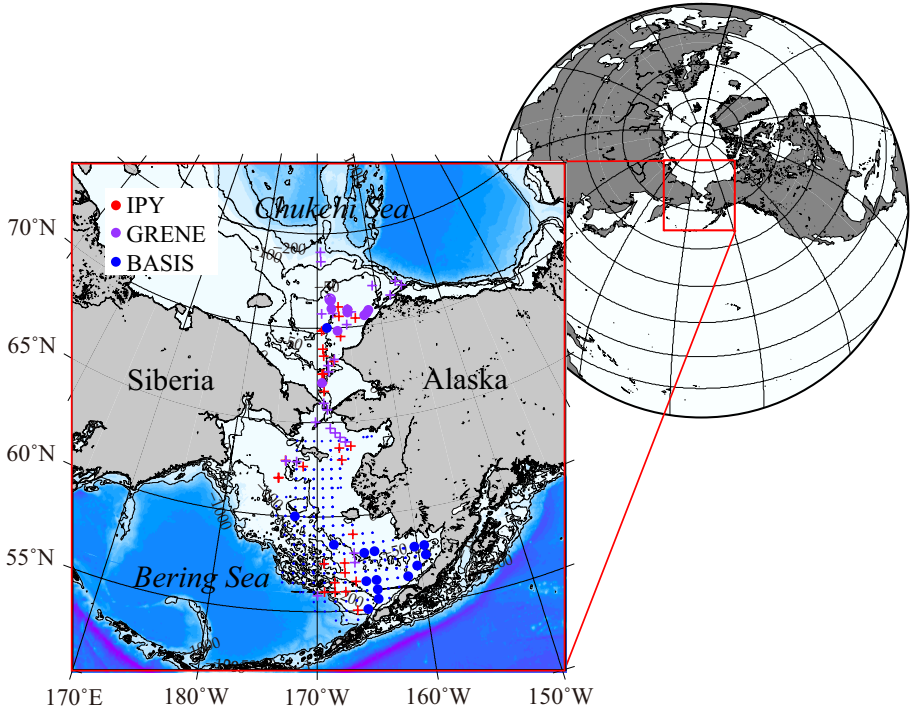

Figure 1. Location of in situ sampling stations for IPY cruises (red), GRENE cruises (violet), and BASIS cruises (blue). Note that stations of daily match-ups between in situ F_L measurements and MODIS Level-2 derived F_L are shown in large circles, and crosses represent where primary productivity measurement was conducted. Contours indicate 100, 200, and 1000 m bathymetry, based on ETOPO-2.

BGD
12, 12611–12651, 2015

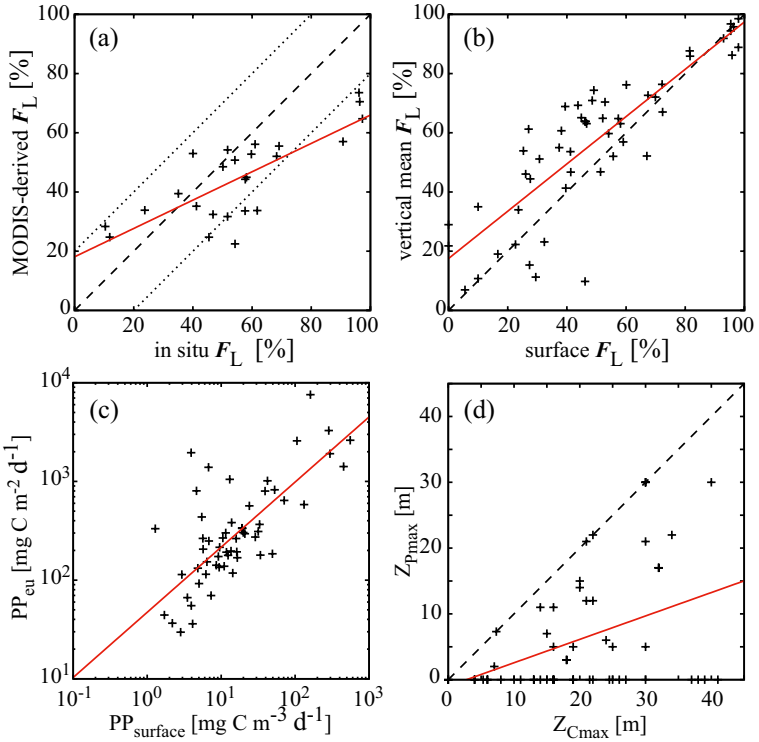

Figure 2. Scatter plot of **(a)** satellite derived F_L vs. in situ observed surface F_L ($r^2 = 0.45$, $p < 0.01$, $N = 25$, RMSE = 25 %), **(b)** in situ vertical mean F_L vs. in situ surface F_L ($r^2 = 0.73$, $p < 0.01$, $N = 63$), **(c)** in situ PP_{eu} vs. in situ surface PP ($r^2 = 0.50$, $p < 0.01$, $N = 56$ in log scale), and **(d)** depth of PP maximum (Z_{Pmax}) vs. depth of chl *a* maximum (Z_{Cmax}). Dashed lines indicates 1 : 1 line, doted lines indicate ±20 % from 1 : 1 (panel **(a)**, and red solid lines represent regression line, respectively.

BGD
12, 12611–12651, 2015

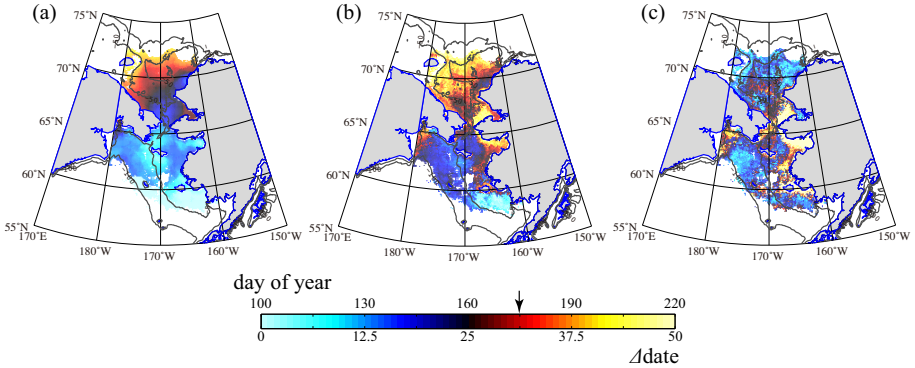

Figure 3. Distribution of 16 year median of **(a)** TSR, **(b)** date of CMAX, and **(c)** date difference between CMAX and TSR. Note that color scale for Fig. 3a and b is indicated on the upper tick marks of the color bar, and the scale of Fig. 3c is indicated on the lower tick marks. The arrow on the color bar denotes the date of summer solstice (day of year = 174). Contours indicate 50, 100 m bathymetry.

BGD
12, 12611–12651, 2015

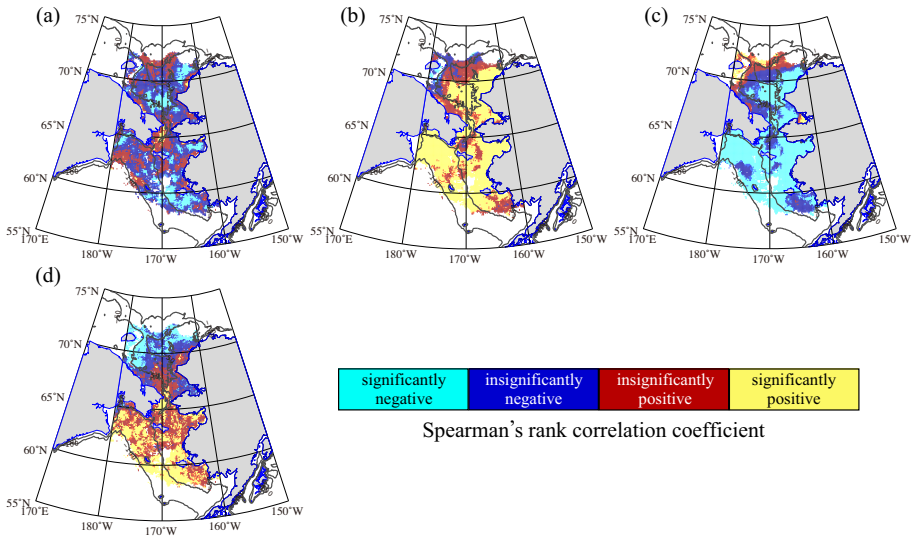

Figure 4. Spatial distribution of Spearman's rank correlation (ρ) between **(a)** F_L during MIZ period and TSR, **(b)** SST during MIZ period and TSR, **(c)** ΔOHC during MIZ period and TSR, and **(d)** PAR during MIZ period and TSR. Yellow indicates significantly positive ρ ($p < 0.05$), red, positive ρ ($p > 0.05$), blue, negative ρ ($p > 0.05$), and light blue, significantly negative ρ ($p < 0.05$). Proportion of the coefficients is listed in Table 2. Contours indicate 50, 100 m bathymetry.

BGD
12, 12611–12651, 2015

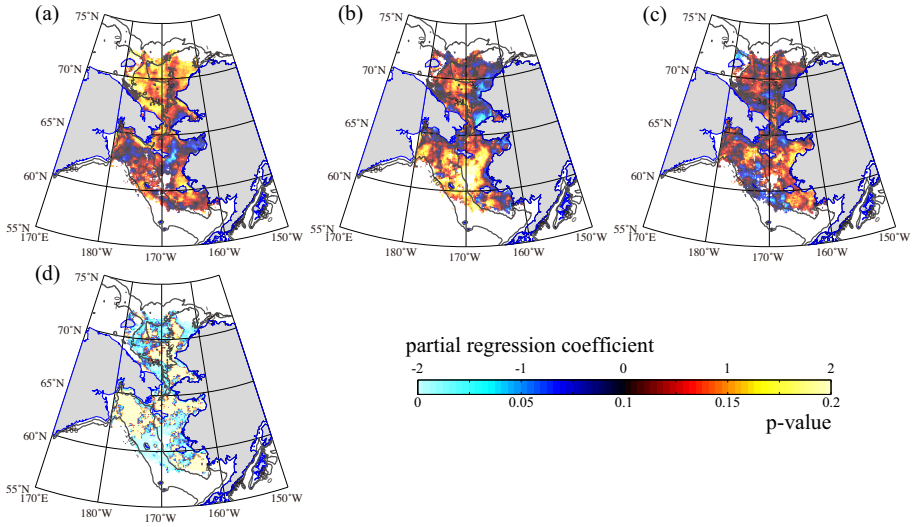

Figure 5. Distribution of the partial regression coefficient from Eq. (7) for **(a)** standardized length of open water period, **(b)** standardized annual median of F_L, and **(c)** standardized annual median of SST. Distribution of p value as the result of the F test for Eq. (7) is shown in Fig. 5d. Note that color scale in Fig. 5a–c is indicated on the upper tick marks on the color bar, and the scale in Fig. 5d is indicated on the lower tick marks. Contours indicate 50, 100 m bathymetry.

BGD
12, 12611–12651, 2015

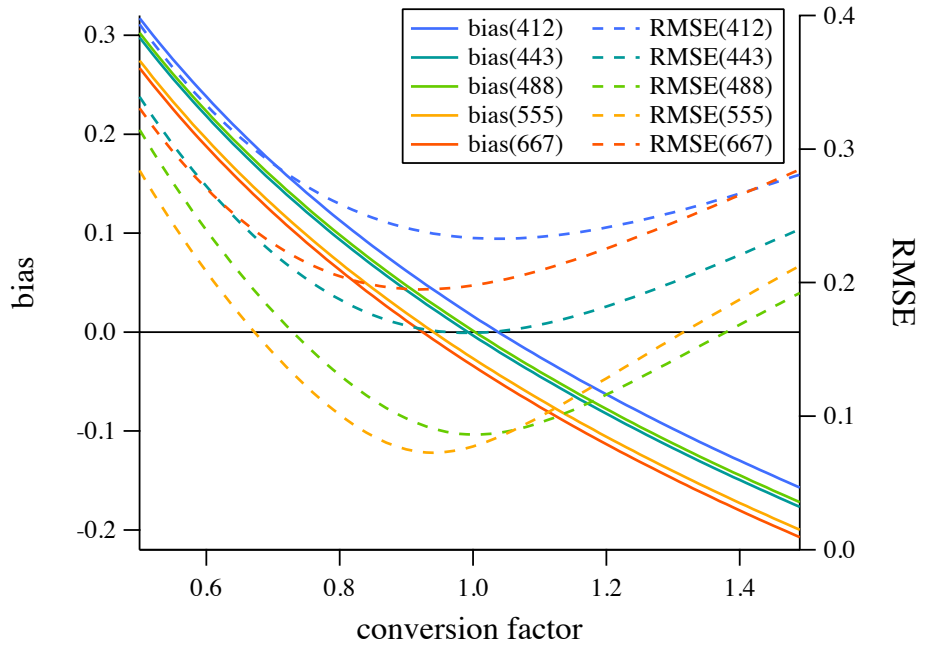

Figure A1. Bias (left axis) and RMSE (right axis) between MODIS-$R_{rs}(\lambda)$ and converted SeaWiFS-$R_{rs}(\lambda)$ to MODIS-$R_{rs}(\lambda)$ as a function of conversion factor. Lines colored in blue, sky blue, green, yellow and red indicate λ = 412, 443, 490, 555, and 667, respectively. The conversion factors for each band were determined as the optimum factor when the bias was equivalent to zero (listed in Table A1). Note that both bias and RMSE was calculated for log-transformed $R_{rs}(\lambda)$.

BGD
12, 12611–12651, 2015

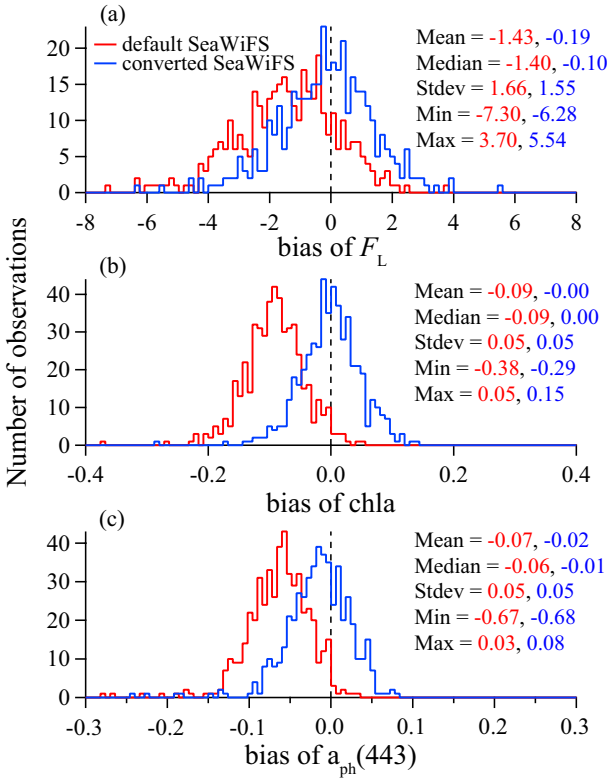

Figure A2. Histograms and statistics of the bias between SeaWiFS and MODIS retrieved **(a)** F_L, **(b)** chl *a*, and **(c)** a_{ph} (443). Red colored lines and statistics denote the results from default SeaWiFS-$R_{rs}(\lambda)$, and blue colored lines and statistics denote the results from converted SeaWiFS-$R_{rs}(\lambda)$. The products were significantly improved ($p < 0.01$) for means (*t* test) and medians (*U* test). Note that biases of chl *a* and $a_{ph}(443)$ were computed for the log-transformed values.

BGD
12, 12611–12651, 2015

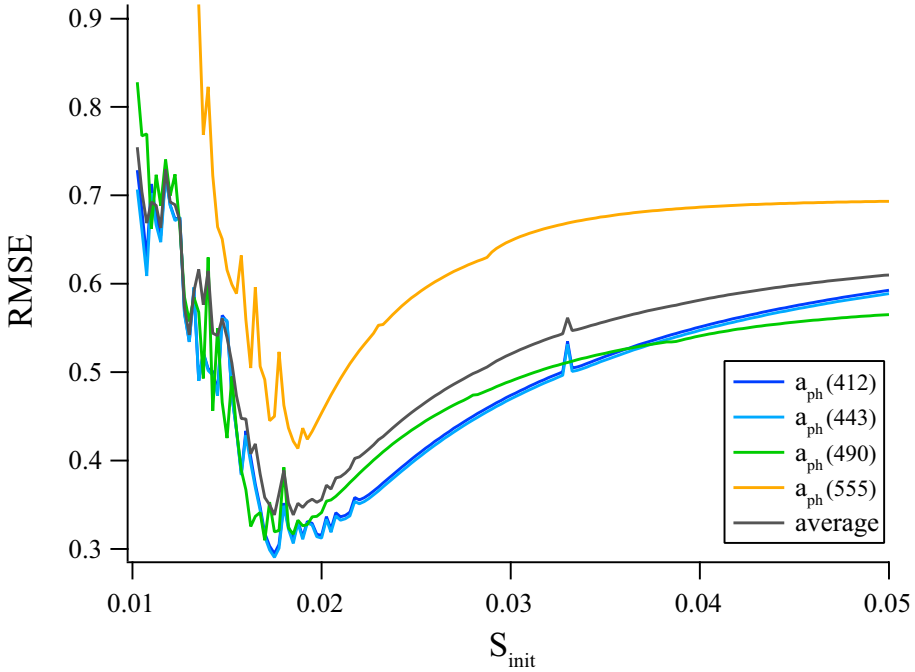

Figure B1. RMSE between in situ $a_{ph}(\lambda)$ and QAA derived $a_{ph}(\lambda)$ as a function of spectral slope of a_{dg} (S_{dg}). Lines colored in blue, sky blue, green, yellow and gray denote $a_{ph}(412)$, $a_{ph}(443)$, $a_{ph}(490)$, $a_{ph}(555)$, and the average of them, respectively. Optimum value of S_{dg} was determined when RMSE for the average became minimum (= 0.019). Note that the RMSEs were calculated for log-transformed $a_{ph}(\lambda)$.

BGD
12, 12611–12651, 2015